

Persistent Homology of Weighted Visibility Graph from Fractional Gaussian Noise

H. Masoomy,¹ B. Askari,¹ M. N. Najafi,^{2,*} and S. M. S. Movahed^{1,†}

¹*Department of Physics, Shahid Beheshti University, 1983969411, Tehran, Iran*

²*Department of Physics, University of Mohaghegh Ardabili, P.O. Box 179, Ardabil, Iran*

In this paper, we utilize persistent homology technique to examine the topological properties of the visibility graph constructed from fractional Gaussian noise (fGn). We develop the weighted natural visibility graph algorithm and the standard network in addition to the global properties in the context of topology, will be examined. Our results demonstrate that the distribution of *eigenvector centrality* and *betweenness centralities* behave as power-law decay. The scaling exponent of *eigenvector centrality* and the moment of *eigenvalue* distribution, M_n , for $n \geq 1$ reveal the dependency on the Hurst exponent, H , containing the sample size effect. We also focus on persistent homology of k -dimensional topological holes incorporating the filtration of simplicial complexes of associated graph. The dimension of homology group represented by *Betti numbers* demonstrates a strong dependency on the Hurst exponent. More precisely, the scaling exponent of the number of k -dimensional topological *holes* appearing and disappearing at a given threshold, depends on H which is almost not affected by finite sample size. We show that the distribution function of *lifetime* for k -dimensional topological holes decay exponentially and corresponding slope is an increasing function versus H and more interestingly, the sample size effect is completely disappeared in this quantity. The persistence entropy logarithmically grows with the size of visibility graph of system with almost H -dependent prefactors.

Keywords: Topological Data Analysis, Persistent Homology, Fractional Gaussian Noise, Weighted Natural Visibility Graph, Topological Persistence, Persistence Entropy

I. INTRODUCTION

A powerful approach to study different types of data sets ranging from point cloud data (PCD), scalar field to complex network (graph), particularly a high-dimensional data is called topological data analysis (TDA) [1–6]. TDA as an application of algebraic topology [7–9] and a branch of computational topology [10], analyzes the shape of high-dimensional complex data in terms of global features (number of connected components, loops, voids, *etc.*) of topological space underlying the data set. In the persistent homology (PH) technique, as a main part of TDA, the topological approximation of phase space of any type of data sets which is called simplicial complex is assigned to the associated data, then topological invariants are computed.

The PH aims to capture topological evolution of data set by varying scale (parameter), and extracts topological invariants of data set in each scale summarizing them in different representations, persistence barcode (PB) [11, 12], persistence diagram (PD) [13, 14], persistence landscape (PL) [15], persistence image (PI) [16], persistence surface (PS) and β -curve, which reveal topological information of data set. Being robust to noise, PH is able to show us the essential features of the systems with high internal degrees of freedom and is capable to classify underlying data sets [17, 18]. The PH technique has attracted much attention due to its vast applications on analyzing complex networks [19–21]. Also it has been

used in various systems (see e.g. [22–31] and references therein).

There are many algorithms to assign a network (graph) to different types of data sets. As an illustration, the *Mapper algorithm* constructing the Reeb graphs (topological networks) from high-dimensional PCD [32–35]. The *visibility graph technique* makes a network so-called visibility graph (VG) for a typical time-series (one-dimensional scalar field). The idea of VG, being a complex network constructed by considering the *visibility* algorithm, proposed by Lacasa *et al* as a novel way to analyze time-series in terms of complex networks language [36]. The associate networks can be examined by various methods [1, 37]. The advantage of this idea is that, one can apply many well-known techniques in networks and even in TDA such as PH for a time-series, helping for classification, discrimination and looking for exotic features hidden in the underlying time-series which could be robust in the presence of noise, trends and irregularities [36–40]. The notion of mapping the time-series to a network has been applied on different topics (see [41–51] and references therein).

As a model containing correlations tuned by one parameter (the Hurst exponent H), the fractional Gaussian noise (fGn) time-series has been intensely investigated by many methods. To quantify the properties of a given self-similar data set or a generic series whose power spectrum behaves as power-law in frequency (wavelength) domain, many methods have been proposed concerning the trends and noises which may affect the observed time-series. Many preceding methods are implemented either in time domain or frequency space. A well-studied method is multi-fractal detrended fluctuation analysis (MF DFA) [52, 53], implemented in various areas (see [54–

* morteza.nattagh@gmail.com

† m.s.movahed@ipm.ir

74] and references therein).

Beyond the weighted auto-correlation notion, the cross-correlation has also been established and utilized in various disciplines [75–81]. Taking into account the higher-order detrended covariance, the multi-fractal detrended cross-correlation analysis (MFDXA) has been introduced [82]. In spite of many advantages brought by mentioned methods, but the impact of more complicated trends and finite size effect have not been diminished completely in many previous approaches [83–88]. In order to eliminate the effect of trend as much as possible, several robust methods have been proposed [64, 86–89]. On the other hand, the finite size of time-series impacts on the accurate estimation of Hurst exponent by some of previous methods [90].

The VG approach which is derived by mapping a time-series into a network is able to represent some interesting results for a typical fGn data [41, 42, 91]. An alternative method to estimate H , can be devoted to graph theoretical algorithm [41]. Despite of huge literature, very little attention has been paid to topological properties of VG associated with a self-similar series.

In this regard, knowing a given time-series belongs to a fGn class, some relevant questions can be raised: i) Does the topological aspect of associated VG depend on the Hurst exponent? ii) What are the effects of sample size, trends and irregularity of fGn signal on the topological properties of VG? iii) How is the multifractality expressed by persistence homology? Motivated by mention questions, we focus on the persistent homology of weighted visibility graph constructed from a typical fGn by using the filtration process and considering higher-order connections (k -cliques ; $k > 2$) in all thresholds (weights) [92, 93], to examine the dependency of relevant results to H and footprint of finite size effect. We show that, in contrast to local statistical features considered in this paper which are less-sensitive to auto-correlation of fGns, the topological features are sensitive to the value of corresponding Hurst exponent and are size-independent. The contribution of trends and irregularity and even determining whether an input data is a fGn signal or not are beyond the scope of current study.

This paper is organized as follows: In the next section we present the network concepts to be used in the paper. The Sec. III is devoted to how VGs are obtained for a time-series. The weight functions are introduced in this section. The numerical results are presented in Sec. IV, which contains two subsections: local statistical properties, and topological properties. We close the paper with a summary and conclusion.

II. NETWORK ANALYSIS

In this paper, we aim to analyze the complex network of the visibility graph constructed from a fractional Gaussian noise (fGn), with an emphasis on the topological aspects. Besides this, we also compute some conventional

statistical properties of mentioned signal. Therefore, it is worthy to introduce and present a short review of these analyzes, referring the interested readers to the relevant references such as [94–96].

A. Statistical Analysis

In this subsection, we introduce some conventional quantities, would be used in the following sections, with a main focus on various centrality measures. Inspired by social network science, the centralities play an important role in identifying the key elements in a typical network, such as the most effective agents (the degree centrality or the eigenvector centrality), the easiest access agent (the closeness centrality), and the betweenness centrality.

Suppose that a network (graph) is represented by $G = (V, E, w)$. Here, $V \equiv \{v_i\}_{i=1}^N$ is node (vertex) set, $E = V \times V \equiv \left\{ e_{ij} = (v_i, v_j) \middle| v_i, v_j \in V \right\}_{i,j=1}^N$ is link (edge) set and $w : E \rightarrow \mathbb{R}$ is a weight function (threshold). Subsequently, the *degree* of i th node, v_i , is the number of nodes straightly connected with underlying node by non-zero weight, and it is denoted by $k_i \equiv \sum_j (1 - \delta_{0, w_{ij}})$. The *degree centrality*, c_i^D , is defined by $\frac{k_i}{N-1}$, which is apparently related directly to how important the underlying node is, since it is the number of agents that have connection with it. An important function concerning this quantity is the degree distribution, $p(k)$, showing the probability distribution function for degree of all nodes in the network

$$p(k) = \frac{1}{N} \sum_{i=1}^N \delta_{k, k_i} \quad (1)$$

The *eigenvector centrality*, c_i^E , is also defined via the eigenvalue equation

$$\lambda c_i^E = \sum_{j=1}^N w_{ij} c_j^E \quad (2)$$

where λ is the eigenvalue. The maximum value of the λ spectrum, i.e. λ_{\max} plays the dominant role in the network properties. The corresponding eigenvectors of which are denoted by $c_{i, \max}^E$ showing the importance of the nodes. To define the *closeness centrality*, let us denote the shortest distance between nodes v_i and v_j by d_{ij} which is assumed to be N when there is no path connecting them (disconnected graphs). Then the *closeness centrality* is defined by

$$c_i^C = \frac{N-1}{\sum_{j=1}^N d_{ij}}, \quad (3)$$

and the *betweenness centrality* is as follows

$$c_i^B = \frac{1}{(N-1)(N-2)} \sum_{j=1, j \neq i}^N \sum_{k=1, k \neq i, j}^N \frac{n_{jk}(i)}{n_{jk}}, \quad (4)$$

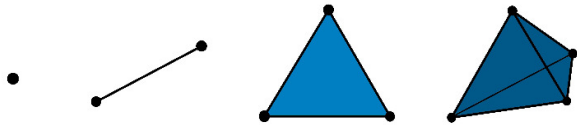


FIG. 1. Low dimensional simplices: 0-simplex (point), 1-simplex (line segment), 2-simplex (filled triangle), 3-simplex (filled tetrahedron).

the n_{jk} is the number of geodesics from v_j to v_k , and $n_{jk}(i)$ is the number of geodesics from v_j to v_k which passing through node v_i . Finally, another interesting quantity which enables us to asses the statistical properties of a network is known as *clustering coefficient* of node v_i . This shows how the first neighbors of node v_i are connected together

$$c_i^{CC} = \frac{2!(k-2)!}{k!} \sum_{j=1}^N \sum_{k=1}^N (1-\delta_{0,w_{ij}})(1-\delta_{0,w_{ik}})(1-\delta_{0,w_{jk}}), \quad (5)$$

which represents the fraction of available triangles in the network. In the upcoming subsection, we will give a brief introduction about algebraic topology.

B. Topological Analysis: Algebraic Topology

In addition to the conventional statistical analysis, introduced in the previous subsection, complex networks exhibit some interesting topological properties. Such properties enable us in classifying the underlying network in a feasible approach. It may utilize to recognize exotic features in data sets. Topology is generally refers to the global features in contrast to geometrical invariants of underlying *objects* or *sets*. Having two spaces represented by X and Y , and they have same local (geometric) features if any relevant features are invariant under *congruence*. While, mentioned spaces are topologically equivalent, if associated features are invariant under *homeomorphisms*. In other words, they are homeomorphic. *Homology theory* plays a crucial role in the mathematical description of the relevant building block of a typical topological space, and reveal the connectedness of underlying space [94–96]. Based on such properties, for the sake of clarity, we will give a brief review on the building blocks of algebraic topology which are useful to set up homology groups.

Simplex: A k -simplex, σ_k , is a convex-hull of any geometrically independent subset, accordingly $\sigma_k \equiv [x_0, x_1, \dots, x_k] \subseteq \mathbb{R}^D$. By this definition, a 0-simplex is a point, a 1-simplex is a segment of a line, a 2-simplex is a filled triangle, a 3-simplex is a filled tetrahedron and so on (Fig. 1).

Face: A l -simplex which is denoted by σ_l , is a subset of k -simplex ($\sigma_l \subseteq \sigma_k$) and it is so-called the l -face of

k -simplex.

Simplicial complex: A simplicial complex, ψ , is a collection of simplices such that: any l -face of any k -simplex of a typical complex ($0 < l < k$), is a member of complex. In addition, the non-empty intersection of any two simplices, σ_k and σ_m , from complex, is a l -face of both simplices. Dimension of a complex is the maximum dimension of all simplices of the complex. According to the definition of complex, one can define k -ordered sub-collection of complex ψ as follows

$$\Sigma_k(\psi) \equiv \left\{ \sigma \in \psi \mid \dim(\sigma) = k \right\}$$

Chain: For a given simplicial complex, a k -chain (k -dimensional chain) is a linear combination of k -simplices of ψ , defined by

$$c_k \equiv \sum_{i=1}^{|\Sigma_k(\psi)|} a_i \sigma_k^{(i)} \quad ; \quad \sigma_k^{(i)} \in \Sigma_k(\psi)$$

where $|\Sigma_k(\psi)|$ corresponds to the cardinality of k -ordered subcollection of complex and the coefficients, a_i s, belong a field, which is usually considered as $\mathbb{F} = \mathbb{Z}_2 \equiv \{0, 1\}$. The collection of all possible k -chains in simplicial complex is called k -chain group as

$$C_k(\psi) \equiv \left\{ c_k \mid c_k = \sum_{i=1}^{|\Sigma_k(\psi)|} a_i \sigma_k^{(i)} ; \sigma_k^{(i)} \in \Sigma_k(\psi), a_i \in \mathbb{F} \right\}$$

Boundary operator: For the simplices in any dimension, the boundary operator ∂_k is an operator mapping σ_k to its boundary according to

$$\partial_k(\sigma_k) \equiv \sum_{j=0}^k (-1)^j [x_0, x_1, \dots, x_{j-1}, x_{j+1}, \dots, x_k] \subseteq \sigma_k$$

Boundary: A k -chain which is the boundary of a $(k+1)$ -chain, is called k -boundary, denoted by b_k . The k -boundary group is the collection of all k -boundaries in complex ψ

$$B_k(\psi) \equiv \left\{ c_k \in C_k(\psi) \mid \exists c_{k+1} \in C_{k+1}(\psi); \partial_{k+1}(c_{k+1}) = c_k \right\} \\ \equiv \left\{ b_k^{(i)} \right\}_i^{|\Sigma_k(\psi)|} \subseteq C_k(\psi)$$

Cycle: A k -chain that has no boundary, is called a k -cycle denoted by z_k as

$$\partial_k(z_k) = \emptyset$$

The k -cycle group is defined as the collection of all k -cycles in complex ψ

$$Z_k(\psi) \equiv \left\{ c_k \in C_k(\psi) \mid \partial_k(c_k) = \emptyset \right\} \\ \equiv \left\{ z_k^{(i)} \right\}_i^{|\Sigma_k(\psi)|} \subseteq C_k(\psi)$$

Since "Boundaries have no boundary.", therefore, we have




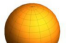


Topological space Betti numbers						
β_0	1	1	1	1	1	1
β_1	0	0	1	0	2	6
β_2	0	0	0	1	1	1

FIG. 2. Betti numbers of some topological spaces: point, line, circle, sphere, torus, 2-torus.

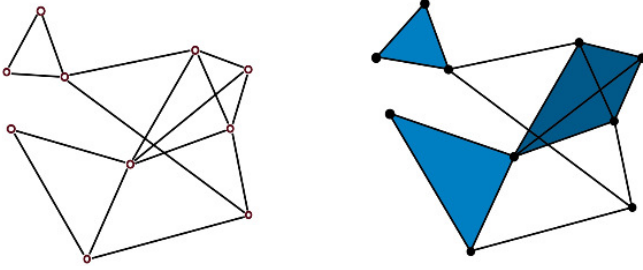


FIG. 3. Clique complex (right) of a typical network (left).

$$\partial_k(b_k) = \partial_k(\partial_{k+1}(c_{k+1})) = \emptyset$$

hence

$$B_k(\psi) \subseteq Z_k(\psi) \subseteq C_k(\psi)$$

Homology group: The k -homology group is defined by the quotient group of the k -cycles group by the k -boundary group

$$H_k(\psi) \equiv Z_k(\psi)/B_k(\psi)$$

The k th *Betti number* of a simplicial complex, denoted by $\beta_k(\psi)$, is a topological invariant which counts number of k -homology class corresponding to the number of k -dimensional holes of complex ψ (Fig. 2)

$$\beta_k(\psi) \equiv \dim(H_k(\psi))$$

Clique (flag) simplicial complex of an unweighted (binary) network, $G = (V, E, w \in \{0, 1\})$, is a simplicial complex, denoted by $\psi^{(G)}$, such that any k -simplex of each dimension in complex corresponds to a $(k+1)$ -clique in the network and vice versa (Fig. 3).

A binary network is a *topological tree*, if and only if, it is topologically holeless in all dimensions. Namely, the associated clique simplicial complex has following property

$$\beta_k(\psi^{(G)}) = \min(\beta_k) = \begin{cases} 1 & ; & k = 1 \\ 0 & ; & k > 1 \end{cases}$$

In the context of topological data analysis (TDA), we are interested in statistical analysis of the structure in data. Generally, in TDA-based analysis, data with any type (point cloud data, scalar field, time-series, network, etc.) when mapped to a weighted simplicial complex

are worked out topologically in terms of the parameters present inherently in the original data, e.g. the weight of links in a weighted network, or the pairwise distance between data points in point cloud data. More precisely, TDA maps parameter-dependent data, $X(w)$, (where w is a typical parameter, like the threshold value for any weighted network) to a weighted simplicial complex, $\psi^X(w)$. Such approach produces the chain group, the cycle group, the boundary group, the homology group and particularly, the k th Betti number [7, 10].

Persistent homology (PH) as a powerful tool of TDA, examines the creation (birth) and destruction (death) of topological invariants associated with homology classes during a mathematical process called filtration [94]. In fact, filtration, ϕ , is a nested sequence of weighted complex $\psi(w)$ which any complex with a distinct weight is a subcollection of any complex with higher weight

$$\phi(\psi(w)) \equiv \left(\psi(w) \mid \forall w' < w'' : \psi(w') \subseteq \psi(w'') \right)_{w_{\min}}^{w_{\max}} \quad (6)$$

More precisely, PH technique enumerates k th Betti number of any subcomplex in ϕ and assigns an ordered tuple $w^{(h_k)} \equiv (w_{\text{birth}}^{(h_k)}, w_{\text{death}}^{(h_k)})$ to existed k -dimensional topological hole. Here $w_{\text{birth}}^{(h_k)}$ and $w_{\text{death}}^{(h_k)}$ are the thresholds for which, h_k appears (birth) and disappears (death) respectively. Since $w_{\text{birth}}^{(h_k)} < w_{\text{death}}^{(h_k)}$, we can define the positive-value quantity $\ell^{(h_k)} \equiv w_{\text{death}}^{(h_k)} - w_{\text{birth}}^{(h_k)}$ as persistency (lifetime) of k -dimensional hole. Persistence barcode (PB) or equivalently persistence diagram (PD) are the famous representations of PH. As an illustration, k -dimensional persistence diagram of weighted complex $\psi(w)$ is a multiset $PD_k(\phi(\psi(w))) \equiv (\mathcal{M}, \mathcal{N})$, where $\mathcal{M} \equiv \left\{ w^{(h_k)} \mid h_k \in H_k(\psi(w)), \psi(w) \in \phi \right\}$ and $\mathcal{N} : \mathcal{M} \rightarrow \mathbb{N}$ is the count function. Inspired by Shannon entropy for a typical state probability, one can define the persistence entropy (PE) of k th PD (PB). To this end, we construct the probability for lifetime of homology classes as

$$p(\ell^{(h_k)}) \equiv \frac{\ell^{(h_k)}}{\mathcal{L}} \quad ; \quad \mathcal{L} \equiv \sum_{w^{(h_k)} \in \mathcal{M}(PD_k)} \ell^{(h_k)}$$

Therefore, the PE for k -dimensional persistent homology is defined by [97–99]:

$$PE_k = - \sum_{w^{(h_k)} \in \mathcal{M}(PD_k)} p(\ell^{(h_k)}) \log p(\ell^{(h_k)}) \quad (7)$$

Relying on previous quantities, we try to characterize the synthetic fGn series.

III. VISIBILITY GRAPH

Among growing applicability of complex networks in many fields and interdisciplinary branches in science [100], a technique has been suggested which converts a time-series to a network, so-called visibility graph

(VG) [36]. Generally, suppose $\{x\} : \{x(t_i), i = 1, \dots, N\}$ represents a real-valued time-series. One can construct a network, so-called visibility graph, denoted by $G = (V, E, w)$, the $V \equiv \{v_i\}_{i=1}^N$ is again node (vertex) set, and E is link (edge) set. The VG is defined by using the bijection as follows

$$f : V \equiv \{v_i\}_{i=1}^N \leftrightarrow T \equiv (t_i)_{i=1}^N ; \quad f(v_i) = t_i \quad (8)$$

and the connections are constructed according to *visibility condition* between the nodes, i.e. the nodes v_i and v_j are connected if the node v_j is visible from the node v_i and vice versa, therefore the resulting graph is undirected (for more details on the properties of VGs, see [36]). In general, there are two ways to construct a network (graph) from a time-series: the horizontal visibility graph (HVG) [39, 101, 102] and the natural visibility graph (NVG) [103–105], the former is more sparse than the latter case and in this work we focus on the NVG. In Fig. 4, we show how a HVG (left panel) and a NVG (right panel) for a synthetic fGn series can be con-

structed. In a binary set up, the corresponding visibility graph chooses the range of the weights from a binary set, $w^{(B)} : E \rightarrow \mathbb{Z}_2 \equiv \{0, 1\}$, e.g. for a binary NVG (BNVG) the weight function can be written according to following relation

$$w_{ij}^{(BN)} \equiv \begin{cases} 1 & ; \quad |f(v_i) - f(v_j)| = 1 \\ \prod_{k=i+1}^{j-1} \Theta(s_{ij} - s_{ik}) & ; \quad |f(v_i) - f(v_j)| > 1 \end{cases} \quad (9)$$

where Θ is the step function, and $s_{ij} \equiv \frac{x(f(v_j)) - x(f(v_i))}{f(v_j) - f(v_i)}$. The argument of the Θ function being positive guarantees that the node v_j is visible from the node v_i and vice versa.

Since the edge in a BNVG has the weight 0 or 1, consequently, making it unsuitable for continuous filtering. Instead, we suggest the weighted version of the natural visibility graph (WNVG), by considering the weight function as follows

$$w_{ij}^{(WN)} \equiv \begin{cases} |s_{ij}| & ; \quad |f(v_i) - f(v_j)| = 1 \\ \left(\prod_{k=i+1}^{j-1} \Theta(s_{ij} - s_{ik}) [s_{ij} - s_{ik}] \right)^{1/(j-i-1)} & ; \quad |f(v_i) - f(v_j)| > 1 \end{cases} \quad (10)$$

There are two factors inside the product. In the second branch of Eq. (10), one is the step function just like the binary graph, and the other is the weight which is proportional to “how visible is the site j from i and vice versa”, i.e. the more distinguishable the data points are in the original time-series, the higher the corresponding weight are in the constructed network. The term $\frac{1}{j-i-1}$ is necessary to make the weights reasonable numbers for comparison reasons. In the absence of this exponent, the more the distance between the nodes are, the higher the corresponding weights are. For both statistical and the topological analysis, we use this weight function which admits continuous filtering.

A. Synthetic Fractional Gaussian Noise

In order to modeling the stochastic fractal processes, Mandelbrot and Van Ness introduced the fractional Brownian motion (fBm) and fractional Gaussian noise (fGn) [106]. The mathematical generalization of the classical random walk and Brownian motion is given by the theory of fBm [106–108]. A 1-dimensional fBm is represented by $B \equiv \{B(t) : t \geq 0\}$, with power-law variance is the fractional Brownian motion (fBm), for which $Var(B(at)) \triangleq Var(a^H B(t)) = a^{2H} Var(B(t))$, where

$H \in (0, 1)$ is called Hurst exponent. For this random force, the Markov property and the stationarity are violated (note that when we have domain Markov property, stationarity and continuity for a time-series, then it should be proportional to a 1-dimensional Brownian motion). A model for generating fBm (denoted by B_H to emphasis on its Hurst exponent H) is a generalization of the Brownian motion which is non-stationary and non-Markov [109, 110], is given by the Holmgren-Riemann-Liouville fractional integral

$$B_H(t) = \frac{1}{\Gamma(H + \frac{1}{2})} \int_0^t (t-s)^{H-\frac{1}{2}} dB(s) \quad (11)$$

where Γ is Gamma function, $dB(s) \equiv B(s+ds) - B(s)$ is the increment of 1-dimensional Brownian motion and it has the following covariance:

$$\langle B_H(t) B_H(s) \rangle = \frac{\sigma^2}{2} \left(|t|^{2H} + |s|^{2H} - |t-s|^{2H} \right), \quad (12)$$

where $\sigma^2 \equiv \langle B(0) \rangle$ and also $\langle B_H \rangle = 0$. The common fBm is retrieved by setting $H = \frac{1}{2}$. The increments, $x_H(t) = \delta_t (B_H(t+\delta t) - B_H(t))$ are known as fractional Gaussian noise (fGn). For $H > \frac{1}{2}$ ($H < \frac{1}{2}$) the corresponding fGn is positively (negatively) correlated, called the superdiffusive (subdiffusive) regime. Throughout this paper, we simulated various fGn with different

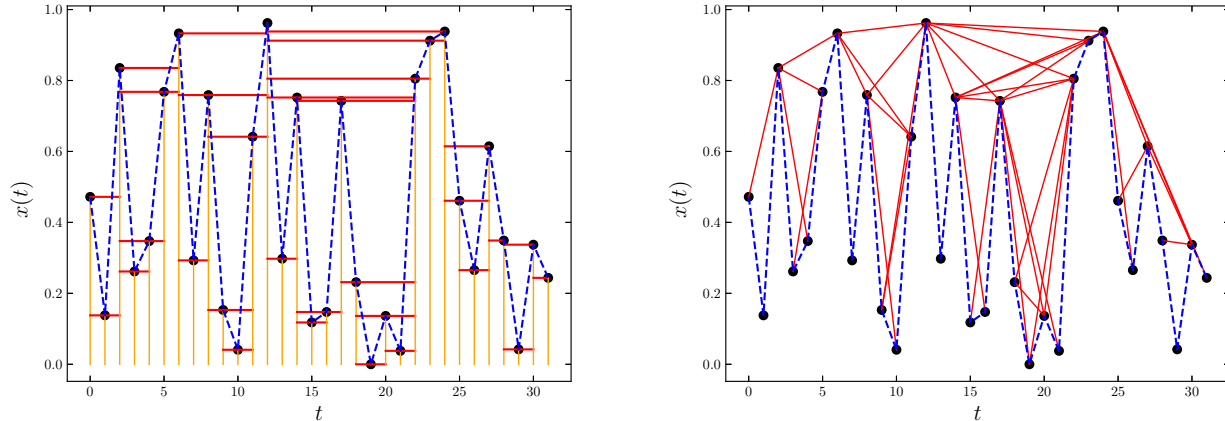


FIG. 4. The schematic representation of making network for a typical data set. The NVG (right panel) and HVG (left panel) of a synthetic fGn with $H = 0.5$ (white-noise). To make more sense, we took the sample size equates to $N = 32$.

self-similar exponents and size. To reduce any bias in nominal Hurst exponent as much as possible, all relevant results are determined by ensemble average over 10^4 realizations generated by our computational algorithm for each H . In addition, we have computed the value of H associated with each synthetic data set by our code based on DFA method [53].

IV. RESULTS

Here we focus on the statistical (next subsection) and topological (the other subsection) properties of the VGs constructed from the fGn time-series, and investigate their behavior with respect to the Hurst exponent H . The networks of sizes $N = 2^7, 2^8, 2^9, 2^{10}, 2^{11}$ and 2^{12} (that a desktop with 128 GB memory is capable to perform matrix operations) are considered and the ensemble averages are performed over 10^4 realizations. The Python toolbox “NetworkX” [111] is employed for the matrix operations on the graphs. In the topological analysis we especially focus on the Betti-0 (represented by the β_0 defined as the number of connected components of the network) and Betti-1 (represented by β_1 defined as the number of loops) features, which are extracted by using “Dionysus” Python package [112]. The persistence statistics, containing the lifetime (the interval between birth and death) of the topological features, and its Shannon entropy are also analyzed.

Each exponent has been estimated by Bayesian statistics accordingly, the $\{\mathcal{D}\}$ and $\{\Upsilon\}$ reveal the data and model free parameters, respectively. The posterior function is defined by

$$\mathcal{P}(\Upsilon|\mathcal{D}) = \frac{\mathcal{L}(\mathcal{D}|\Upsilon)\mathcal{P}(\Upsilon)}{\int \mathcal{L}(\mathcal{D}|\Upsilon)\mathcal{P}(\Upsilon)d\Upsilon} \quad (13)$$

where \mathcal{L} is the likelihood and $\mathcal{P}(\Upsilon)$ is the prior probability function containing all information concerning model parameters. Here we adopt the top-hat function for prior function whose window’s size depends on expected range of corresponding exponent. Taking into account the central limit theorem, the functional form of likelihood becomes multivariate Gaussian, i.e. $\mathcal{L}(\mathcal{D}|\Upsilon) \sim \exp(-\chi^2/2)$. The χ^2 for determining the best-fit value for the scaling exponent reads as

$$\chi^2(\Upsilon) \equiv \Delta^\dagger \cdot C^{-1} \cdot \Delta \quad (14)$$

where Δ is a column vector whose elements are determined by difference between computed value and theoretical form for each measure and C is the corresponding covariance matrix. Finally, the best fit value of considering exponent is computed by maximizing the likelihood probability distribution and associated error-bar is given by

$$68.3\% = \int_{-\sigma_\Upsilon}^{+\sigma_\Upsilon} \mathcal{L}(\mathcal{D}|\Upsilon)d\Upsilon \quad (15)$$

Subsequently, we report the best value of the scaling exponent at a 1σ confidence interval as $\Upsilon_{-\sigma_\Upsilon}^{+\sigma_\Upsilon}$.

A. Local Statistical Properties

By local properties, we mean the properties that are node-dependent, and are not necessarily globally defined. It has been confirmed that, the distribution function of the node degree of VGs of the fBms and fGns is power-law $\mathcal{P}(k) \propto k^{-\gamma}$ with the exponent $\gamma(H) = 3 - 2H$ and $\gamma(H) = 5 - 2H$, respectively [36, 41]. In this subsection, we perform our calculations for the WNVG, introduced for the first time in this paper.

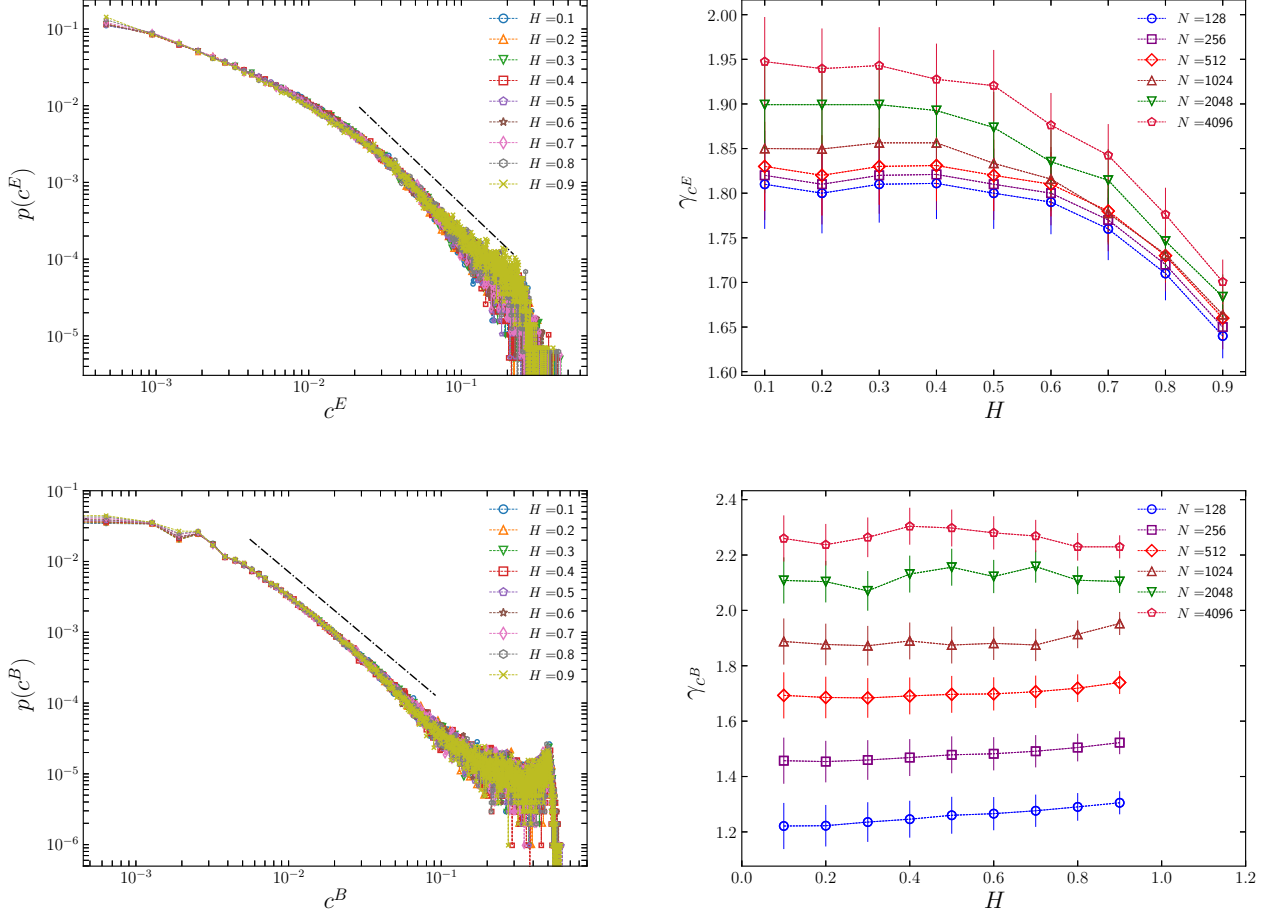


FIG. 5. Probability distribution function of local features of WNVGs constructed from fGns for various Hurst exponent. The upper left panel is $p(c^E)$ while the lower left panel shows the probability distribution of betweenness centrality for $N = 2^{10}$. The right panels illustrate the corresponding scaling exponents for the proper range indicated by dashed line as a function of Hurst exponent for various sizes.

The probability distribution function of *eigenvector* (c^E) and *betweenness* (c^B) centralities are indicated in Fig. 5, in terms of H for WNVGs. The upper and lower right panels in this plot show the exponents of $p(y) \sim y^{-\gamma_y}$, where $y \equiv c^E, c^B$ computed for the proper range in which the probability distribution function reveals the scaling behavior (noticed by dashed-dot line). The γ_{c^E} is almost constant for the negatively correlated regime ($0 < H < \frac{1}{2}$) and is a decreasing function of H for the positively correlated regime ($\frac{1}{2} < H < 1$). The γ_{c^B} is however constant for all H values, showing that the *betweenness centrality* is not affected by changing H .

Also Fig. 6 illustrates the probability distribution function of *closeness centrality* (c^C) and *eigenvalue* for various H exponent for WNVGs with different sizes. As shown in this plot, the $p(c^C)$ does not depend on H (upper left panel of Fig. 6). The full spectrum of the *eigenvalues* (Eq. (2)) is illustrated in the lower left

panel of Fig. 6. It shows the activity, or equivalently the strength of the weights of the network [113]. We see that the impact of H is changing the range of spectrum and by increasing Hurst exponent the range of spectrum for WNVGs become tight. This phenomenon can be understood recalling that, as a well-known fact, correlations (obtained by increasing H) smooths the underlying time-series, causing the corresponding network has more link with low weight. For more smoothed time-series, the typical slopes for associated WNVG become low, leading to lower weights according to Eq. (10), and equivalently making shorter range for the distribution of λ . The right panels in Fig. 6 indicate different moments for $p(c^C)$ (upper panel) and $p(\lambda)$ (lower panel). The solid and dashed lines correspond to M_2 and M_3 , respectively. Let us summary the results of this section:

1- The distribution of the *eigenvector* and *betweenness centralities* behave as power-law. The scaling exponent

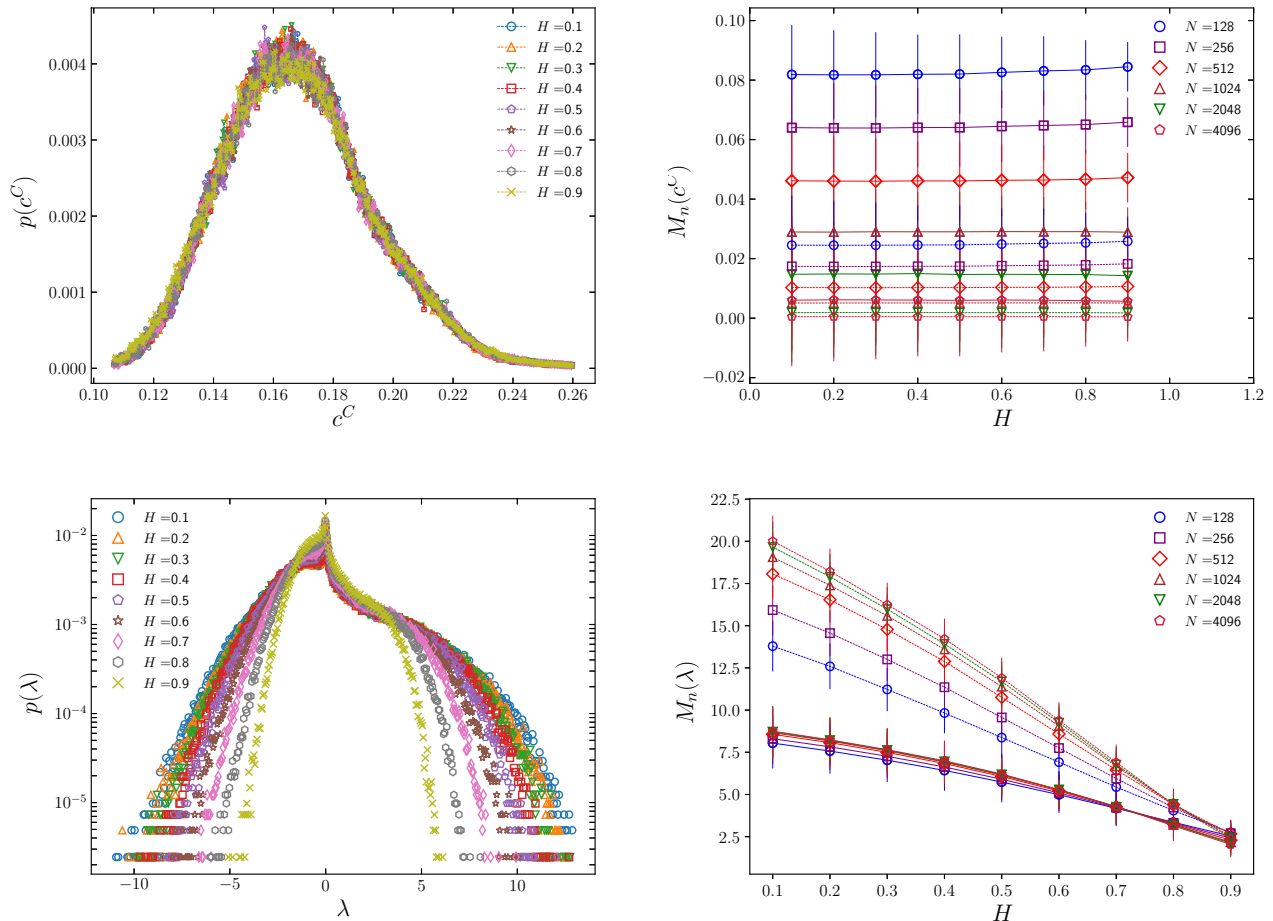


FIG. 6. Probability distribution function of local features of WNVGs constructed from fGns for various Hurst exponent. The upper left panel is $p(c^C)$ while the lower left panel shows the probability distribution of eigenvalue for $N = 2^{10}$. The right panels illustrate the corresponding moments, M_n , for $n = 2$ (solid line) and $n = 3$ (dashed line) versus H . Different symbols are taken for various sizes.

for $p(c^B)$ is almost independent of H , while the γ_{c^E} behaves as decreasing function in terms of Hurst exponent. Precisely, for $H < 0.5$ the corresponding scaling exponent is almost constant versus H and it decreases by increasing Hurst exponent for $H > 0.5$.

2- Increasing correlation (i.e. increasing H) makes the time-series smooth, leading to more dense networks and shifts the weights to lower values, making the width of the distribution function of the eigenvalues smaller.

3- Fig. 5, confirm that the local observables are weakly dependent on the value of H , but in the next subsection, we will show that the dependence of the topological observables on H are more considerable and more interestingly, the impact of sample size is almost diminished.

B. Topological Properties

In this subsection, we rely on the statistics of topological measures to examine the structures embedded in the networks constructed by visibility graph mapping. For any given value of Hurst exponent, the associated BNVGs of fGns are topological tree, therefore, the BNVGs, are topologically equivalent to each others. In another word, various BNVGs are homeomorphic for different H according to homeomorphism theorem. Consequently, we only focus on topological aspects of WNVGs.

Generally, in the homology theory, the computable algebraic invariants of topological space are introduced. The *Betti numbers* are among the topological invariants counting the number of k -homology class. Such quantities represent the number of k -dimensional topological holes of associated simplicial complex produced by different methods such as clique simplicial complex strat-

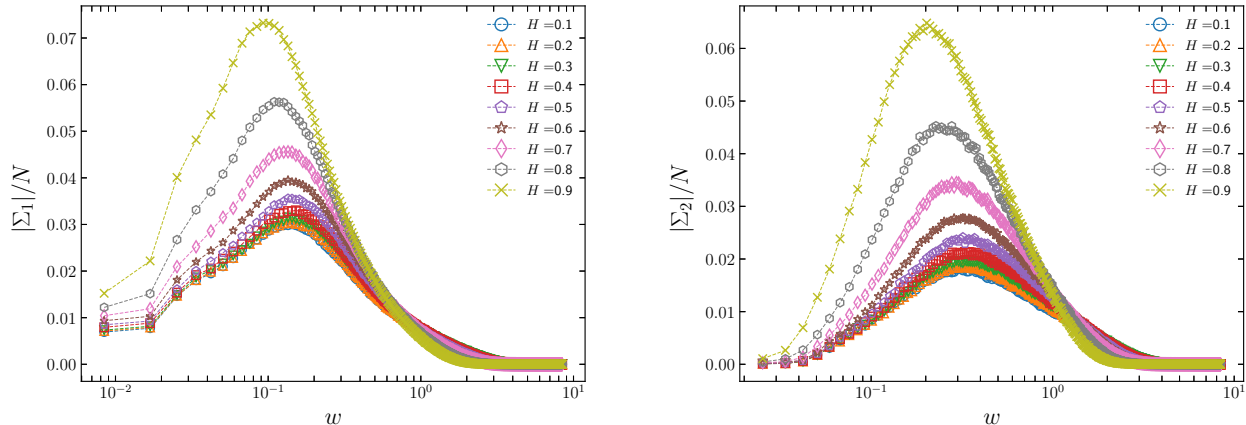


FIG. 7. Statistics of weighted clique complex simplices. The number of 1-dimensional (left panel) and 2-dimensional (right panel) simplices of weighted simplicial complex of WNVGs associated with fGns computed at the threshold. Different symbols are devoted to various Hurst exponents.

egy. In principle, the *Betti numbers* can be modified and become as a more simple measures known as *Euler characteristics*. Our purpose here is that, by computing topological invariants of underlying sets we attempt to distinguish between various series. To this end, we carry out the filtration approach on the WNVGs produced for each synthetic fGn and then, we will compute the set of *Betti numbers*, β_k ($k = 0$ corresponds to connected components, $k = 1$ is associated with loops and so on). The filtration at (continuous) weight, w , is simply performed as follows: we connect nodes v_i and v_j if $w_{ij} < w$. It is worth noting that all values reported for relevant quantities have been determined by ensemble average as mentioned before.

For the first step, we compute the normalized number of simplices of weighted clique simplicial complex at the threshold for the WNVGs associated with fGns. Fig. 7 shows the normalized numbers of links (1-simplices), $|\Sigma_1|$, and triangles (2-simplices), $|\Sigma_2|$, for different Hurst exponents. By increasing H , the abundance of links and triangles grow at low thresholds, on the contrary, by going to the high threshold regime, mentioned statistics decrease under the same action. This result is compatible with our expectation for WNVG of a typical fGn constructed by Eq.(10). For low H , the underlying signals has more fluctuations leading to have more roughness, consequently, the abundance of weights effectively moves to high w , while for high value of Hurst exponent, the signal achieves more smoothed fluctuations yielding to get higher abundance of links with low weights. As depicted in Fig. 7, the threshold for which the $|\Sigma_1|$ and $|\Sigma_2|$ reach to their maximum is weakly dependent to Hurst exponent. Here a question arises: which characteristic threshold can separates “low” weights from the “high” one in the underlying network?. To answer this question, we look at lines for different H crossing each other

more and less in a same point, and we called it as w^* . At mentioned threshold, the abundance of links or triangles with $w < w^*$ increase by increasing H , and on the contrary, for $w > w^*$ regime, the abundance of links or triangles are reducing when the value of Hurst exponent increases. At this threshold, the value of $|\Sigma_1|(w^*)$ is nearly independent to H , while for $|\Sigma_2|$, we have a small range of w , such crossing happens. Nevertheless, we interpret w^* as the crossover point, the scale which separates the low and high weights.

Now, we are going to evaluate topological measures. The upper panel of Fig. 8 indicates the β_0 (the number of connected components) as a function of filtration parameter (threshold) for clique complexes of WNVGs produced for various time-series with different values of Hurst exponent. To reduce the effect of sample size, we divide the Betti numbers by the samples size and called it as *normalized Betti numbers*. By increasing the value of Hurst exponent, the normalized β_0 versus threshold decrease. Namely, the number of connected components in the network decreases with increasing H (the graphs become more steep). Interestingly, the slope of normalized β_0 as a function of w is different for different H , consequently, the WNVGs of fGn sets reaches to connected regime (path-connected), $\beta_0 = 1$, (in the upper left panel of Fig. 8, we take $N = 1024$) by different rates and at different thresholds, w_0 . The upper right panel of Fig. 8 represents the value of w_0 as a function of Hurst exponent for different networks size. As depicted in mentioned panel, the value of w_0 behaves as a sample size dependent quantity and by increasing H , such dependency becomes negligible.

We define the $\beta_k^{(\text{birth})}(w)$ and $\beta_k^{(\text{death})}(w)$ as the number of k -dimensional holes that born and die at a given threshold, w , respectively. It turns out that $\beta_0^{(\text{birth})} = 0$

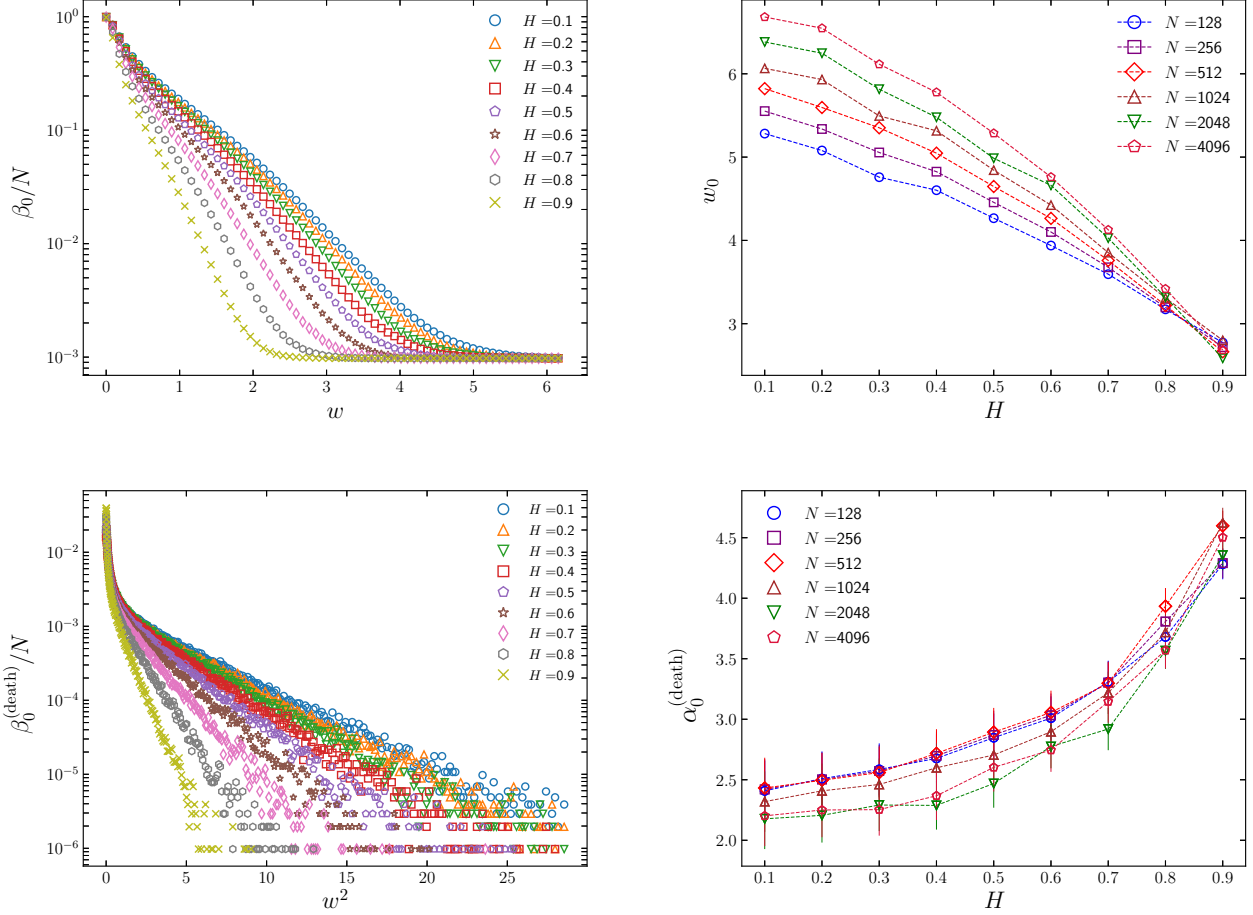


FIG. 8. Upper left panel illustrates the normalized β_0 -curve for clique complexes of WNVGs associated with fGns of various Hurst exponent versus threshold. The upper right panel indicates the w_0 as a function of H . Lower left panel corresponds to the normalized $\beta_0^{(\text{death})}$ as a function of w^2 in semi-log scale (see the text) for various Hurst exponent as a function of threshold. Lower right panel indicates the value of $\alpha_0^{(\text{death})}$ as a function of Hurst exponent.

for $w > 0$, since at $w = 0$ the underlying network has N connected components, therefore, all connected components born at $w = 0$. The lower left panel of Fig. 8 illustrates the $\beta_0^{(\text{death})}/N$ as a function of w^2 in the semi-log plot. As shown in this plot, one of the proper fitting function to describe the normalized $\beta_0^{(\text{death})}$ is given by $\beta_0^{(\text{death})}(w) \sim \exp(-\alpha_0^{(\text{death})} w^2)$ for $2 \lesssim w^2 \lesssim w_{\text{max}}^2$, where the value of w_{max} depends on the H value. The $\alpha_0^{(\text{death})}$ depends on Hurst exponent as increasing function and it behaves as an almost independent function on size of series (lower right panel of Fig. 8).

The upper left panel of Fig. 9 is devoted to β_1/N for various Hurst exponents. As we expect, for trivial threshold, $w = 0$, we have N connected components ($\beta_0 = N$) and therefore the number of loops is identically zero. By increasing the threshold, the higher value of Hurst exponent leads to more rapid in the increasing rate of β_1 . On

the other hand, for the high enough value of threshold, again the underlying data set behaves as a topological tree without any topological loops. Therefore, the normalized β_1 goes asymptotically to zero and such descending is more rapid for higher H . We also determine the lowest non-trivial threshold for which, there is no loop in underlying network denoted by w_1 , and depict this threshold versus H for different samples size in the upper right panel of Fig. 9. The w_1 is also size-dependent quantity. Comparing the β_0/N and β_1/N demonstrate that the by increasing threshold value, the WNVGs of fGn series reach to loop-less regime ($\beta_1 = 0$) before appearing the connected regime (for which $\beta_0 = 1$), irrespective to Hurst exponent, i.e. $w_0(H) > w_1(H)$. The quantities $\beta_1^{(\text{birth})} \propto \exp[-\alpha_1^{(\text{birth})} w]$, $\beta_1^{(\text{death})} \propto \exp[-\alpha_1^{(\text{death})} w]$ in semi-log plots versus thresholds and corresponding slopes are illustrated in the middle and the lower panels of Fig. 9, respectively. The $\alpha_1^{(\text{birth})}$ and $\alpha_1^{(\text{death})}$ are

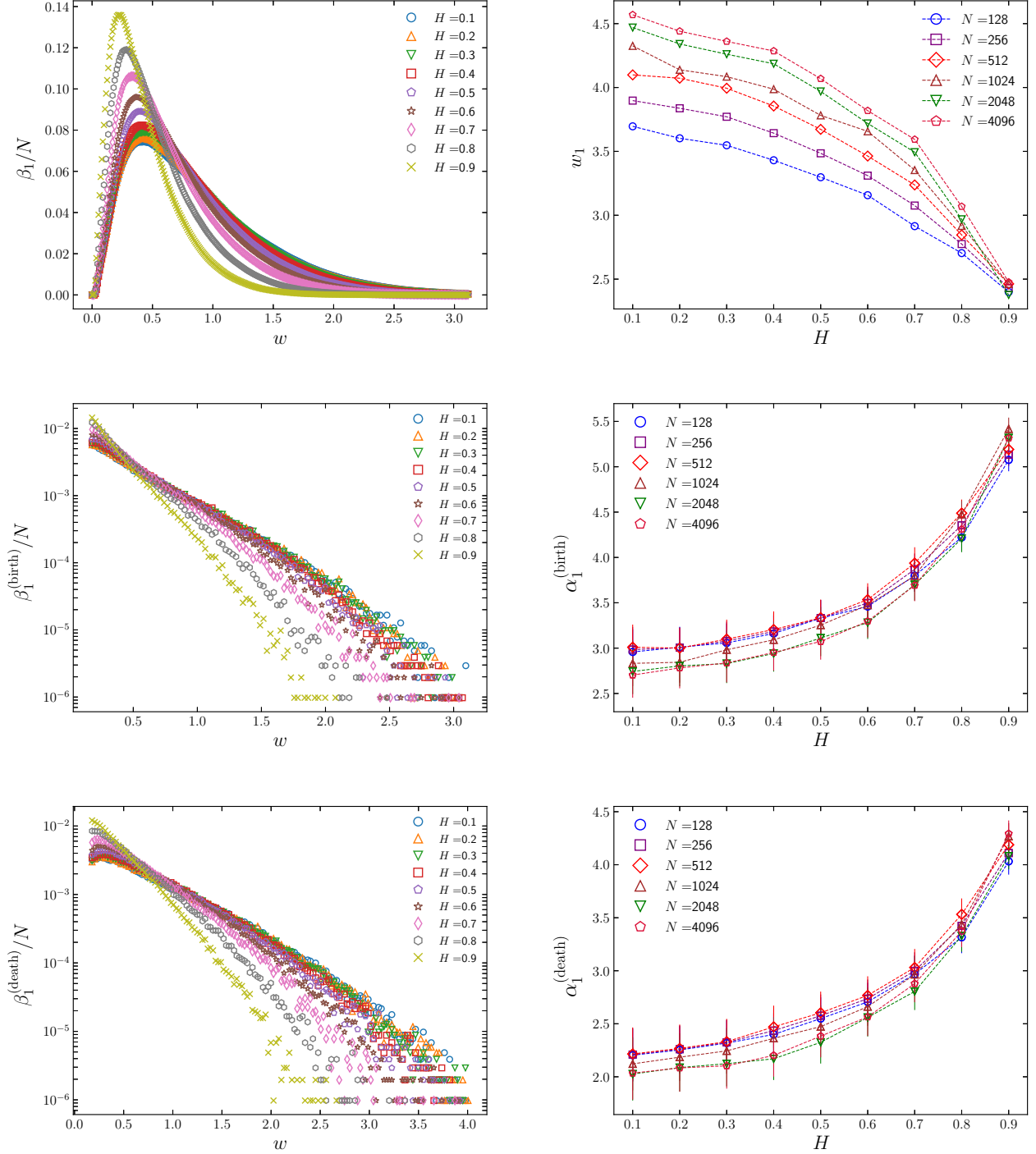


FIG. 9. Upper left panel shows the normalized β_1 -curve for clique complexes of WNVGs associated with fGns of various Hurst exponent versus threshold, while, upper right panel indicates the w_1 as a function of H for different length of data set. The distribution of persistence diagram versus birth-axis as a function of threshold. The middle right panel represents the corresponding coefficient of $\beta_1^{(\text{birth})}$ in terms of threshold known as $\alpha_1^{(\text{birth})}$ as a function of Hurst exponent. The lower panels are the same as middle just for dying 1-hole statistics. In this plot for computing β_1 , we took $N = 1024$.

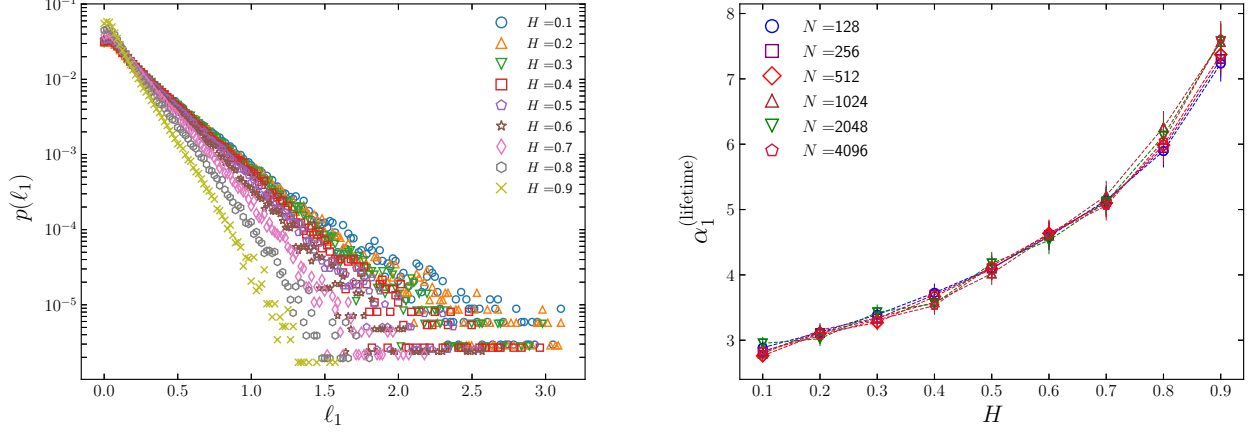


FIG. 10. The probability distribution of lifetime for 1-dimensional holes is depicted in left panel. Different symbols correspond to various H . This diagram has been obtained by doing ensemble average. Right panel is associated with the $\alpha_1^{(\text{lifetime})}$ exponent for different sizes represented by different symbols.

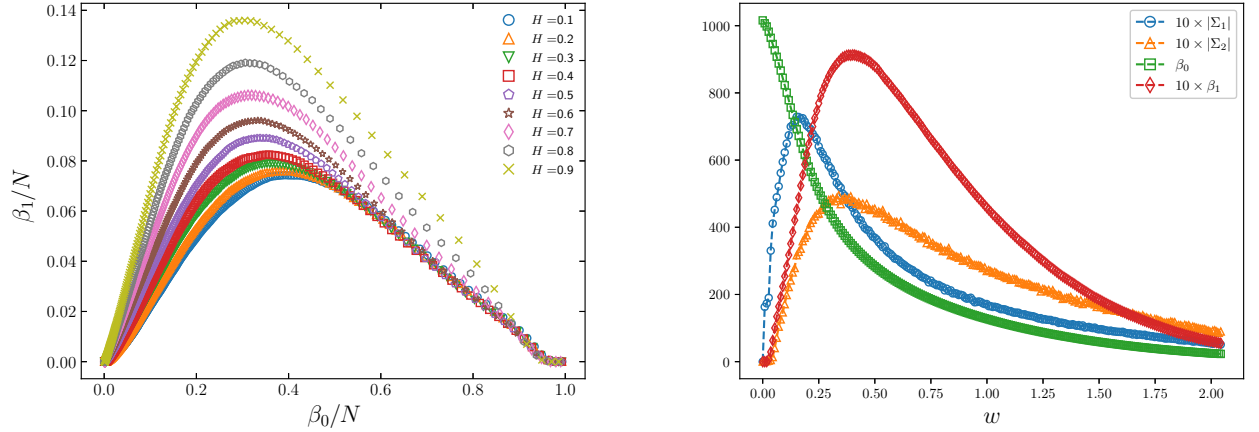


FIG. 11. Left panel illustrates the trajectory of β -vector of weighted clique simplicial complex derived by filtration process of WNVG associated with fGn with different values of Hurst exponent. Right panel indicates the number of 1-simplices (links), number of 2-simplices (triangles), number of 0-holes (connected components) and number of 1-holes (loops) for fGn series with $H = 0.5$. We considered $N = 1024$. For convenient, we multiplied the $|\Sigma_1|$, $|\Sigma_2|$ and β_1 by factor 10.

almost size-independent and they grow by increasing H .

Another interesting property to assess is the probability distribution of lifetime for 1-holes which is difference between the death and birth thresholds of a typical measure in a 1-homology class. The left panel of Fig. 10 shows the probability distribution of topological 1-dimensional holes lifetime, ℓ_1 , for various synthetic data sets with different values for Hurst exponent. Our results confirm that $p(\ell_1) \propto \exp[-\alpha_1^{(\text{lifetime})}\ell_1]$. The H -dependency of $\alpha_1^{(\text{lifetime})}$ for various systems sizes is depicted in the right panel of Fig. 10. This result confirms that, $\alpha_1^{(\text{lifetime})}$ can be considered as a robust measure for determining

the Hurst exponent of fGn signal which is not affected by sample size even compared to $\alpha_0^{(\text{death})}$, $\alpha_1^{(\text{birth})}$ and $\alpha_1^{(\text{death})}$.

The trajectory of β -vector (β -curve) of weighted clique simplicial complex of WNVGs associated with fGns is also a sensitive criterion to reveal H -dependency. The overall behavior of mentioned trajectory does not depend on sample size during filtration process (the left panel of Fig. 11). By increasing H the peak positions move to left showing that higher H values favor smaller β_0 s and higher β_1 s as discussed above.

To make more complete our investigation, regarding the comparison of different topological measures, we de-

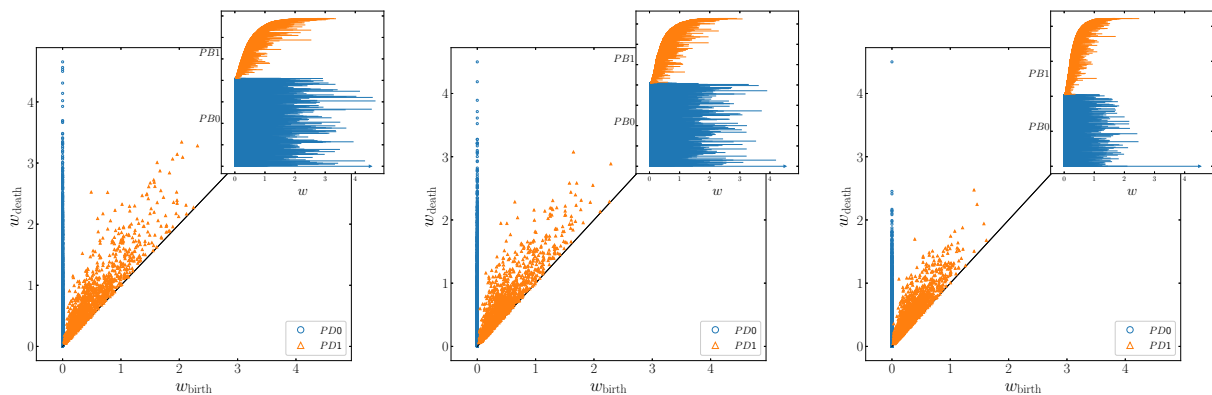


FIG. 12. From left to right are the persistence diagram and persistence barcode (inset) of weighted clique complex of WNVG corresponding to fGn with $H = 0.2$ (anti-correlated noise), $H = 0.5$ (uncorrelated noise) and $H = 0.8$ (correlated noise), respectively. The blue circle and orange triangle symbols are considered for the 0-dimensional and 1-dimensional homology generators, respectively.

pict $|\Sigma_1|$ (1-simplex), $|\Sigma_2|$ (2-simplex), β_0 (connected components) and β_1 (loops) as a function of threshold, for $H = 0.5$, in the right panel of Fig. 11. Each symbols has been computed by ensemble average on different sample size. The maximum value of $|\Sigma_2|$ and β_1 take place almost at the same threshold, while the peak of $|\Sigma_1|$ is different, taking place at w which is approximately half the one for $|\Sigma_2|$ and β_1 . We verify that mentioned treatments are almost independent to Hurst exponent.

Fig. 12 indicates the persistence diagram (PD) and persistence barcode (PB) for three type of fGn signals for $H = 0.2$ (anti-correlated), $H = 0.5$ (un-correlated) and $H = 0.8$ (correlated). The open circle and triangle symbols correspond, respectively to the 0- and 1-homology groups in a persistence diagram for WNVGs of fGn. Each symbol depicts a pair $(w_{\text{birth}}, w_{\text{death}})$ of a k -dimensional hole. As expected, all 0-holes born in $w_{\text{birth}} = 0$, and also always $w_{\text{death}} > w_{\text{birth}}$. In the barcode representation (inset plot), the horizontal lines (blue lines for $k = 0$ and orange lines for $k = 1$) start and end on the threshold values that k -dimensional holes born and die respectively.

The associated persistence entropies (PEs) defined by Eq. (7) are obtained using the persistence diagram. The upper and middle panels of Fig. 13 depict the PE_0 and PE_1 , as a function of sample size in semi-log scale, respectively. We compute persistence entropy for all available Hursts exponent values represented by different symbols. Our results demonstrate that $PE_k = \mathcal{A}_k(H) \log N$ for $k = 0, 1$. The behavior of pre-factor, \mathcal{A}_k versus H is represented in the lower panel of Fig. 13. The \mathcal{A}_0 is almost an increasing function versus Hurst exponent, while the \mathcal{A}_1 becomes constant.

V. SUMMARY AND CONCLUDING REMARKS

In this paper, we used the persistent homology technique to examine the visibility graph (VG) constructed from fractional Gaussian noise (fGn), characterized by Hurst exponent H . To this end, we developed a method to derive weighted visibility graph associated with a time-series. The statistical properties of the model were analyzed using the standard network measures. Our results revealed power-law behaviors for probability distribution function of *eigenvector* and *betweenness centralities* in the proper range of corresponding quantities (left panels of Fig. 5). The scaling exponent of *betweenness centrality* did not depend on H , while the γ_{cE} depends on Hurts exponent for $H > 0.5$ and it almost remained constant for anti-correlated regime (right panels of Fig. 5).

The probability distribution function of *closeness centrality* and associated moments were independent from H . Increasing the correlation results in to have more dense networks and shifts the weights to lower values, making the width of the distribution function of the eigenvalues to be more tight. The $M_n(\lambda)$ behaved as H -dependent quantity. The higher order of moments showed a weak dependency on sample size (Fig. 6).

In the second part, we considered the topological properties of synthetic fGn. The normalized number of simplices (1-simplex and 2-simplex) for data sets with different H the abundance of links and triangles grow at low thresholds when we increase the H . The threshold for which the $|\Sigma_1|$ and $|\Sigma_2|$ reach to their maximum is weakly dependent to Hurst exponent. We also defined a characteristic threshold for separating “low” from “high” weights. The value of $|\Sigma_1|(w^*)$ was nearly independent on H , while for $|\Sigma_2|$, we has a small range of w , such crossing happens. The decreasing rate of Betti-0 which is a representative for the number of connected components with respect to threshold increase

by increasing H . The threshold value for which the underlying WNVG reaches to connected regime (path-connected), w_0 indicated a H -dependency. Our result confirmed that, the value of $\alpha_0^{(\text{death})}$ which is the coefficient of $\beta_0^{(\text{death})}(w) \sim \exp(-\alpha_0^{(\text{death})}w^2)$ depends on Hurst exponent and interestingly it is almost size independent (Fig. 8). The statistics of 1-holes analyzed and we showed that the w_1 showing vanishing threshold for β_1 was H -dependent and it contained the sample size effect. The $\alpha_1^{(\text{birth})}$ and $\alpha_1^{(\text{death})}$ revealed the proper criteria for measuring Hurst exponent (Fig. 9).

The probability distribution of lifetime of 1-hole confirmed that the corresponding coefficient represented by $\alpha_1^{(\text{lifetime})}$ is an increasing function versus H emphasizing that, the sample size effect is completely diminished in this quantity. Consequently, for a self-similar time-series in the absent of trends, the $\alpha_1^{(\text{lifetime})}$ can be a reliable measure for estimating Hurst exponent even for small sample size irrespective to value of H (Fig. 10).

The persistence pairs (PPs) in persistence diagram (PD) and persistence barcode (PB) for weighted clique complex of WNVG which are indicators of persistent homology have been computed and by increasing the value of Hurst exponent are shrink to origin of coordinate (Fig. 12). We also computed persistence entropies (PEs) for 0-homology and 1-homology groups. Both quantities depend on sample size as expected and the corresponding slopes in semi-log scale were almost H -dependent (Fig. 13).

Finally, we emphasize that, the exponents of the local (statistical) observables depend weakly on H , whereas the exponents of global (topological) observables are almost strongly H -dependent. The footprint of sample size on the $\alpha_1^{(\text{lifetime})}$ is completely diminished.

In this paper, we have not verified that whether the persistent homology (PH) technique is capable to recognize the underlying time-series is a self-similar set or not. Indeed, this purpose is beyond the scope of this paper. In addition, it could be interesting to examine the effect of trends and irregularity which may occur in the wide range of events in the nature in the context of TDA and more precisely via persistent homology approach and we left them for future research. Above analysis can be done on different phenomena ranging from cosmology, astrophysics, economy to biology [73, 114–117]

Acknowledgment: The authors are really grateful to Marco Piangerelli for his notice on TDA as starting point in this research. The numerical simulations were carried out on the computing cluster of the University of Mohaghegh Ardabili.

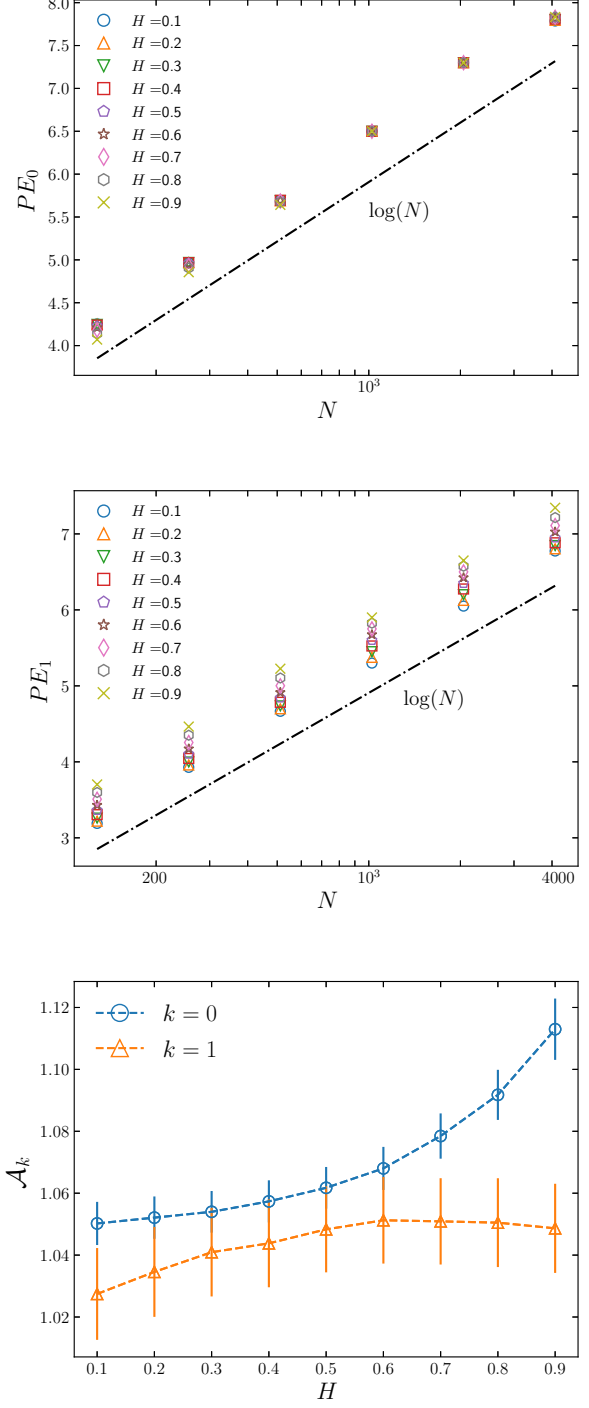


FIG. 13. The upper panel indicates the persistence entropy for 0-homology group, PE_0 , while, the middle is associated with PE_1 for 1-hole as a function of sample size in the semi-log scale. Different symbols correspond to various values of Hurst exponent. The lower panel shows the pre-factor of persistence entropy as a function of H computed by ensemble average.

-
- [1] H. Edelsbrunner, D. Letscher, and A. Zomorodian, in *Proceedings 41st annual symposium on foundations of computer science* (IEEE, 2000) pp. 454–463.
- [2] A. Zomorodian and G. Carlsson, *Discrete & Computational Geometry* **33**, 249 (2005).
- [3] A. J. Zomorodian, *Topology for computing*, Vol. 16 (Cambridge university press, 2005).
- [4] G. Carlsson, *Bulletin of the American Mathematical Society* **46**, 255 (2009).
- [5] A. Zomorodian, *Advances in applied and computational topology* **70**, 1 (2012).
- [6] L. Wasserman, *Annual Review of Statistics and Its Application* **5**, 501 (2018).
- [7] M. Nakahara, *Geometry, topology and physics* (CRC Press, 2003).
- [8] J. R. Munkres, *Elements of algebraic topology* (CRC Press, 2018).
- [9] A. Hatcher, *Algebraic topology* (, 2005).
- [10] H. Edelsbrunner and J. Harer, *Computational topology: an introduction* (American Mathematical Soc., 2010).
- [11] R. Ghrist, *Bulletin of the American Mathematical Society* **45**, 61 (2008).
- [12] G. Carlsson, A. Zomorodian, A. Collins, and L. J. Guibas, *International Journal of Shape Modeling* **11**, 149 (2005).
- [13] A. Patel, *Journal of Applied and Computational Topology* **1**, 397 (2018).
- [14] R. L. Belton, B. T. Fasy, R. Mertz, S. Micka, D. L. Millman, D. Salinas, A. Schenfisch, J. Schupbach, and L. Williams, arXiv preprint arXiv:1805.10716 (2018).
- [15] P. Bubenik and P. Dłotko, *Journal of Symbolic Computation* **78**, 91 (2017).
- [16] H. Adams, T. Emerson, M. Kirby, R. Neville, C. Peterson, P. Shipman, S. Chepushtanova, E. Hanson, F. Motta, and L. Ziegelmeier, *The Journal of Machine Learning Research* **18**, 218 (2017).
- [17] F. Chazal and B. Michel, arXiv preprint arXiv:1710.04019 (2017).
- [18] E. Munch, *Journal of Learning Analytics* **4**, 47 (2017).
- [19] D. H. Serrano, J. Hernández-Serrano, and D. S. Gómez, *Chaos, Solitons & Fractals* **137**, 109839 (2020).
- [20] M. Saggari, O. Sporns, J. Gonzalez-Castillo, P. A. Bandettini, G. Carlsson, G. Glover, and A. L. Reiss, *Nature communications* **9**, 1 (2018).
- [21] A. E. Sizemore, J. E. Phillips-Cremens, R. Ghrist, and D. S. Bassett, *Network Neuroscience* **3**, 656 (2019).
- [22] C. M. Topaz, L. Ziegelmeier, and T. Halverson, *PLoS one* **10**, e0126383 (2015).
- [23] M. Offroy and L. Duponchel, *Analytica chimica acta* **910**, 1 (2016).
- [24] Y. Umeda, *Information and Media Technologies* **12**, 228 (2017).
- [25] P. Pranav, H. Edelsbrunner, R. Van de Weygaert, G. Vegter, M. Kerber, B. J. Jones, and M. Wintraecken, *Monthly Notices of the Royal Astronomical Society* **465**, 4281 (2017).
- [26] A. Cole and G. Shiu, *Journal of High Energy Physics* **2019**, 54 (2019).
- [27] W. Elbers and R. v. d. Weygaert, *Monthly Notices of the Royal Astronomical Society* **486**, 1523 (2019).
- [28] M. Gidea and Y. Katz, *Physica A: Statistical Mechanics and its Applications* **491**, 820 (2018).
- [29] K. Almgren, M. Kim, and J. Lee, *Entropy* **19**, 360 (2017).
- [30] C.-C. Liu, W.-S. E. Chen, C.-C. Lin, H.-C. Liu, H.-Y. Chen, P.-C. Yang, P.-C. Chang, and J. J. Chen, *Nucleic acids research* **34**, 4069 (2006).
- [31] S. Siddiqui, A. Shikotra, M. Richardson, E. Doran, D. Choy, A. Bell, C. D. Austin, J. Eastham-Anderson, B. Hargadon, J. R. Arron, *et al.*, *Journal of Allergy and Clinical Immunology* **142**, 1457 (2018).
- [32] M. Carriere, B. Michel, and S. Oudot, *The Journal of Machine Learning Research* **19**, 478 (2018).
- [33] J. Hu, D. Hong, and X. X. Zhu, *IEEE Transactions on Geoscience and Remote Sensing* **57**, 9025 (2019).
- [34] D. Ristovska and P. Sekuloski, *Mathematical Modeling* **3**, 79 (2019).
- [35] J. L. Nielson, J. Paquette, A. W. Liu, C. F. Guandique, C. A. Tovar, T. Inoue, K.-A. Irvine, J. C. Gensel, J. Kloke, T. C. Petrossian, *et al.*, *Nature communications* **6**, 1 (2015).
- [36] L. Lacasa, B. Luque, F. Ballesteros, J. Luque, and J. C. Nuno, *Proceedings of the National Academy of Sciences* **105**, 4972 (2008).
- [37] A.-L. Barabási *et al.*, *Network science* (Cambridge university press, 2016).
- [38] L. Lacasa, A. Nunez, É. Roldán, J. M. Parrondo, and B. Luque, *The European Physical Journal B* **85**, 217 (2012).
- [39] Z.-K. Gao, Q. Cai, Y.-X. Yang, W.-D. Dang, and S.-S. Zhang, *Scientific reports* **6**, 35622 (2016).
- [40] R. V. Donner, Y. Zou, J. F. Donges, N. Marwan, and J. Kurths, *New Journal of Physics* **12**, 033025 (2010).
- [41] L. Lacasa, B. Luque, J. Luque, and J. C. Nuno, *EPL (Europhysics Letters)* **86**, 30001 (2009).
- [42] X.-H. Ni, Z.-Q. Jiang, and W.-X. Zhou, *Physics Letters A* **373**, 3822 (2009).
- [43] R. John and M. John, *Advances in Water Resources* **134**, 103429 (2019).
- [44] L. Telesca, M. Lovallo, S. Aggarwal, P. Khan, and B. Rastogi, *Pure and Applied Geophysics* **173**, 125 (2016).
- [45] G. Ghimire, N. Jadidoleslam, W. Krajewski, and A. Tsonis, 2020.00017 (2020).
- [46] S. Bhaduri and D. Ghosh, *Clinical EEG and neuroscience* **46**, 218 (2015).
- [47] J. Wang, C. Yang, R. Wang, H. Yu, Y. Cao, and J. Liu, *Physica A: Statistical Mechanics and its Applications* **460**, 174 (2016).
- [48] Z.-G. Yu, V. Anh, R. Eastes, and D. Wang, *Nonlinear Processes in Geophysics* **19**, 657 (2012).
- [49] Y. Long, *Physica A: Statistical Mechanics and its Applications* **392**, 3374 (2013).
- [50] A. Braga, L. Alves, L. Costa, A. Ribeiro, M. De Jesus, A. Tateishi, and H. Ribeiro, *Physica A: Statistical Mechanics and its Applications* **444**, 1003 (2016).
- [51] R. V. Donner and J. F. Donges, *Acta Geophysica* **60**, 589 (2012).
- [52] C.-K. Peng, S. Havlin, H. E. Stanley, and A. L. Goldberger, *Chaos: an interdisciplinary journal of nonlinear science* **5**, 82 (1995).
- [53] J. W. Kantelhardt, S. A. Zschiegner, E. Koscielny-

- Bunde, S. Havlin, A. Bunde, and H. E. Stanley, *Physica A: Statistical Mechanics and its Applications* **316**, 87 (2002).
- [54] J. W. Kantelhardt, arXiv preprint arXiv:0804.0747 (2008).
- [55] A. Bashan, R. Bartsch, J. W. Kantelhardt, and S. Havlin, *Physica A: Statistical Mechanics and its Applications* **387**, 5080 (2008).
- [56] M. S. Movahed and E. Hermanis, *Physica A: Statistical Mechanics and its Applications* **387**, 915 (2008).
- [57] S. Hajian and M. S. Movahed, *Physica A: Statistical Mechanics and its Applications* **389**, 4942 (2010).
- [58] P. C. Ivanov, A. Yuen, B. Podobnik, and Y. Lee, *Physical Review E* **69**, 056107 (2004).
- [59] Y. Liu, P. Gopikrishnan, H. E. Stanley, *et al.*, *Physical review e* **60**, 1390 (1999).
- [60] M. Ausloos, N. Vandewalle, P. Boveroux, A. Minguet, and K. Ivanova, *Physica A: Statistical Mechanics and its Applications* **274**, 229 (1999).
- [61] P. C. Ivanov, A. Yuen, B. Podobnik, and Y. Lee, *Physical Review E* **69**, 056107 (2004).
- [62] P. Ferreira, A. Dionísio, and S. Movahed, *Physica A: Statistical Mechanics and its Applications* **486**, 730 (2017).
- [63] M. S. Movahed, G. Jafari, F. Ghasemi, S. Rahvar, and M. R. R. Tabar, *Journal of Statistical Mechanics: Theory and Experiment* **2006**, P02003 (2006).
- [64] J. Hu, J. Gao, and X. Wang, *Journal of Statistical Mechanics: Theory and Experiment* **2009**, P02066 (2009).
- [65] G. Jafari, P. Pedram, and L. Hedayatifar, *Journal of Statistical Mechanics: Theory and Experiment* **2007**, P04012 (2007).
- [66] H. D. Jennings, P. C. Ivanov, A. d. M. Martins, P. da Silva, and G. Viswanathan, *Physica A: Statistical Mechanics and its Applications* **336**, 585 (2004).
- [67] M. S. Movahed, F. Ghasemi, S. Rahvar, and M. R. R. Tabar, *Physical Review E* **84**, 021103 (2011).
- [68] S. Kimiagar, M. S. Movahed, S. Khorram, S. Sobhanian, and M. R. R. Tabar, *Journal of Statistical Mechanics: Theory and Experiment* **2009**, P03020 (2009).
- [69] Z. Xiao-Yan, L. Zong-Hua, and T. Ming, *Chinese Physics Letters* **24**, 2142 (2007).
- [70] F. Soares, M. M. Freire, M. Pereira, F. Janela, and J. Seabra, in *2009 IEEE Pacific Rim Conference on Communications, Computers and Signal Processing (IEEE, 2009)* pp. 677–681.
- [71] F. Soares, I. Sousa, F. Janela, J. Seabra, M. Pereira, and M. M. Freire, in *2010 IEEE International Workshop on Medical Measurements and Applications (IEEE, 2010)* pp. 161–164.
- [72] L. Zunino, D. Gulich, G. Funes, and A. Ziad, *Optics letters* **39**, 3718 (2014).
- [73] I. Eghdami, H. Panahi, and S. Movahed, *The Astrophysical Journal* **864**, 162 (2018).
- [74] R. Shidpour and S. Movahed, *Physica A: Statistical Mechanics and its Applications* **508**, 757 (2018).
- [75] B. Podobnik and H. E. Stanley, *Physical review letters* **100**, 084102 (2008).
- [76] B. Podobnik, I. Grosse, D. Horvatić, S. Ilic, P. C. Ivanov, and H. E. Stanley, *The European Physical Journal B* **71**, 243 (2009).
- [77] B. Podobnik, Z.-Q. Jiang, W.-X. Zhou, and H. E. Stanley, *Physical Review E* **84**, 066118 (2011).
- [78] X.-Y. Qian, Y.-M. Liu, Z.-Q. Jiang, B. Podobnik, W.-X. Zhou, and H. E. Stanley, *Physical Review E* **91**, 062816 (2015).
- [79] G. F. Zebende, *Physica A: Statistical Mechanics and its Applications* **390**, 614 (2011).
- [80] G. Zebende, M. Da Silva, and A. Machado Filho, *Physica A: Statistical Mechanics and its Applications* **392**, 1756 (2013).
- [81] L. Kristoufek, *Physica A: Statistical Mechanics and its Applications* **431**, 124 (2015).
- [82] W.-X. Zhou *et al.*, *Physical Review E* **77**, 066211 (2008).
- [83] K. Hu, P. C. Ivanov, Z. Chen, P. Carpena, and H. E. Stanley, *Physical Review E* **64**, 011114 (2001).
- [84] Z. Chen, P. C. Ivanov, K. Hu, and H. E. Stanley, *Physical review E* **65**, 041107 (2002).
- [85] J. W. Kantelhardt, E. Koscielny-Bunde, H. H. Rego, S. Havlin, and A. Bunde, *Physica A: Statistical Mechanics and its Applications* **295**, 441 (2001).
- [86] R. Nagarajan and R. G. Kavasseri, *Chaos, Solitons & Fractals* **26**, 777 (2005).
- [87] R. Nagarajan and R. G. Kavasseri, *International Journal of Bifurcation and Chaos* **15**, 1767 (2005).
- [88] R. Nagarajan and R. G. Kavasseri, *Physica A: Statistical Mechanics and its Applications* **354**, 182 (2005).
- [89] C. Chianca, A. Ticona, and T. Penna, *Physica A: Statistical Mechanics and its Applications* **357**, 447 (2005).
- [90] L. Xu, P. C. Ivanov, K. Hu, Z. Chen, A. Carbone, and H. E. Stanley, *Physical Review E* **71**, 051101 (2005).
- [91] M. G. Ravetti, L. C. Carpi, B. A. Gonçalves, A. C. Frery, and O. A. Rosso, *PloS one* **9**, e108004 (2014).
- [92] A. E. Sizemore, C. Giusti, A. Kahn, J. M. Vettel, R. F. Betzel, and D. S. Bassett, *Journal of computational neuroscience* **44**, 115 (2018).
- [93] L. Torres, A. S. Blevins, D. S. Bassett, and T. Eliassirad, arXiv preprint arXiv:2006.02870 (2020).
- [94] H. Edelsbrunner and J. Harer, *Computational topology: an introduction* (American Mathematical Soc., 2010).
- [95] G. Rote and G. Vegter, in *Effective Computational Geometry for curves and surfaces* (Springer, 2006) pp. 277–312.
- [96] A. Zomorodian, *Algorithms and theory of computation handbook* **2** (2009).
- [97] E. Merelli, M. Rucco, P. Sloot, and L. Tesei, *Entropy* **17**, 6872 (2015).
- [98] M. Rucco, F. Castiglione, E. Merelli, and M. Pettini, in *Proceedings of ECCS 2014* (Springer, 2016) pp. 117–128.
- [99] N. Atienza, R. Gonzalez-Diaz, and M. Rucco, *Journal of Intelligent Information Systems* **52**, 637 (2019).
- [100] L. d. F. Costa, O. N. Oliveira Jr, G. Travieso, F. A. Rodrigues, P. R. Villas Boas, L. Antikeira, M. P. Viana, and L. E. Correa Rocha, *Advances in Physics* **60**, 329 (2011).
- [101] B. A. Gonçalves, L. Carpi, O. A. Rosso, and M. G. Ravetti, *Physica A: Statistical Mechanics and its Applications* **464**, 93 (2016).
- [102] W.-J. Xie and W.-X. Zhou, *Physica A: Statistical Mechanics and its Applications* **390**, 3592 (2011).
- [103] M. Zheng, S. Domanskyi, C. Piermarocchi, and G. I. Mias, bioRxiv (2020).
- [104] Y. Yang, J. Wang, H. Yang, and J. Mang, *Physica A: Statistical Mechanics and its Applications* **388**, 4431 (2009).
- [105] M. Ahmadi, H. Adeli, and A. Adeli, *Journal of neural transmission* **117**, 1099 (2010).

- [106] B. B. Mandelbrot and J. W. Van Ness, *SIAM review* **10**, 422 (1968).
- [107] C. Kahane and J.-P. Kahane, *Some random series of functions*, Vol. 5 (Cambridge University Press, 1993).
- [108] J. Beran, *Statistics for long-memory processes*, Vol. 61 (CRC press, 1994).
- [109] I. S. Reed, P. Lee, and T.-K. Truong, *IEEE Transactions on Information Theory* **41**, 1439 (1995).
- [110] D. P. Huy, *Vietnam Journal of Mathematics* **31** (2003).
- [111] <https://networkx.org/>.
- [112] Dmitriy, (<https://mrzv.org/software/dionysus2/>).
- [113] S. A. Moosavi, A. Montakhab, and A. Valizadeh, *Scientific reports* **7**, 1 (2017).
- [114] Y. Akrami, M. Ashdown, J. Aumont, C. Baccigalupi, M. Ballardini, A. Banday, R. Barreiro, N. Bartolo, S. Basak, K. Benabed, *et al.*, *Astronomy & Astrophysics* **641**, A4 (2020).
- [115] A. Vafaei Sadr, M. Farhang, S. Movahed, B. Bassett, and M. Kunz, *Monthly Notices of the Royal Astronomical Society* **478**, 1132 (2018).
- [116] P. Ferreira, A. Dionísio, and S. Movahed, *Physica A: Statistical Mechanics and its Applications* **486**, 730 (2017).
- [117] R. Palaniappan, *Biological signal analysis* (BookBoon, 2011).